Centrosome-intrinsic mechanisms modulate centrosome integrity during fever

Anastassiia Vertii, Wendy Zimmerman, Maria Ivshina, and Stephen Doxsey
Program in Molecular Medicine, University of Massachusetts Medical School, Worcester, MA 01605

ABSTRACT **The centrosome is critical for cell division, ciliogenesis, membrane trafficking, and immunological synapse function. The immunological synapse is part of the immune response, which is often accompanied by fever/heat stress (HS). Here we provide evidence that HS causes deconstruction of all centrosome substructures primarily through degradation by centrosome-associated proteasomes. This renders the centrosome nonfunctional. Heat-activated degradation is centrosome selective, as other nonmembranous organelles (midbody, kinetochore) and membrane-bounded organelles (mitochondria) remain largely intact. Heat-induced centrosome inactivation was rescued by targeting Hsp70 to the centrosome. In contrast, Hsp70 excluded from the centrosome via targeting to membranes failed to rescue, as did chaperone inactivation. This indicates that there is a balance between degradation and chaperone rescue at the centrosome after HS. This novel mechanism of centrosome regulation during fever contributes to immunological synapse formation. Heat-induced centrosome inactivation is a physiologically relevant event, as centrosomes in leukocytes of febrile patients are disrupted.**

Monitoring Editor
Yixian Zheng
Carnegie Institution

Received: Mar 18, 2015
Revised: Jul 30, 2015
Accepted: Aug 4, 2015

INTRODUCTION

The centrosome is known best for its ability to nucleate and organize microtubule (MT) arrays in interphase and mitosis. It also functions as a platform for ciliogenesis, membrane trafficking, organization of the immunological synapse, and other cellular processes (Doxsey *et al.*, 2005; Stinchcombe *et al.*, 2006; Andrés-Delgado *et al.*, 2013). The immunological synapse is an important feature of the immune response, a complex reaction often accompanied by the febrile condition (fever; Hanson, 1997). Elevated levels of molecular chaperones such as Hsp70 are a hallmark of the heat stress (HS) response and serve to protect cells from stress and ensure protein quality control in the cell (Bukau *et al.*, 2006; Okiyoneda *et al.*, 2010; Hartl *et al.*, 2011; Calloni *et al.*, 2012; Willmund *et al.*, 2013). Hsp70 protects centrosome integrity during HS (Vidair *et al.*, 1993; Brown *et al.*, 1996), but it is unclear whether this is a global protective effect of Hsp70 on cell metabolism or a specific function at the centrosome itself. The beneficial effect of Hsp70 on membranous organelles was demonstrated for heat-stressed nuclei (Kose *et al.*, 2012) and lysosomes, where Hsp70 corrected the disease features of Niemann–Pick disease (Kirkegaard *et al.*, 2010). On the basis of these observations, we reasoned that Hsp70 may stabilize centrosomes after HS. Here we determine the mechanisms of centrosome disruption and recovery during HS and investigate centrosome integrity in cells of febrile individuals and in HS cells.

RESULTS

Elevated body temperature causes centrosome damage

To test for centrosome damage during fever, we first analyzed centrosomal γ-tubulin levels in leukocytes from febrile (body temperature >38.2°C [101°F]) and normothermic individuals (body temperature 36.6–37°C [97–98.6°F]; Figure 1A). Centrosomes of febrile individuals showed a dramatic loss in γ-tubulin compared with normothermic controls. A similar effect was observed in cultured human retinal pigment epithelial (hRPE) cells treated with fever-mimicking or previously reported (Brown *et al.*, 1996) short-term HS (Figure 1, B and C). The febrile condition is a complex response, involving exogenous (e.g., lipopolysaccharide [LPS]) and endogenous (cytokines) pyrogens (Dinarello, 2004). We tested the contribution of these pyrogens to centrosome disruption using primary cultured mouse macrophages—immune cells that are responsive to

This article was published online ahead of print in MBoC in Press (http://www.molbiolcell.org/cgi/doi/10.1091/mbc.E15-03-0158) on August 12, 2015.

Address correspondence to: Stephen Doxsey (stephen.doxsey@umassmed.edu).

Abbreviations used: HS, heat shock; Hsp70, heat shock protein 70; IL-1, interleukin 1; IS, immunological synapse; LPS, lipopolysaccharide; MB, midbody; MT, microtubules; PCM, pericentriolar material; PCNT, pericentrin.

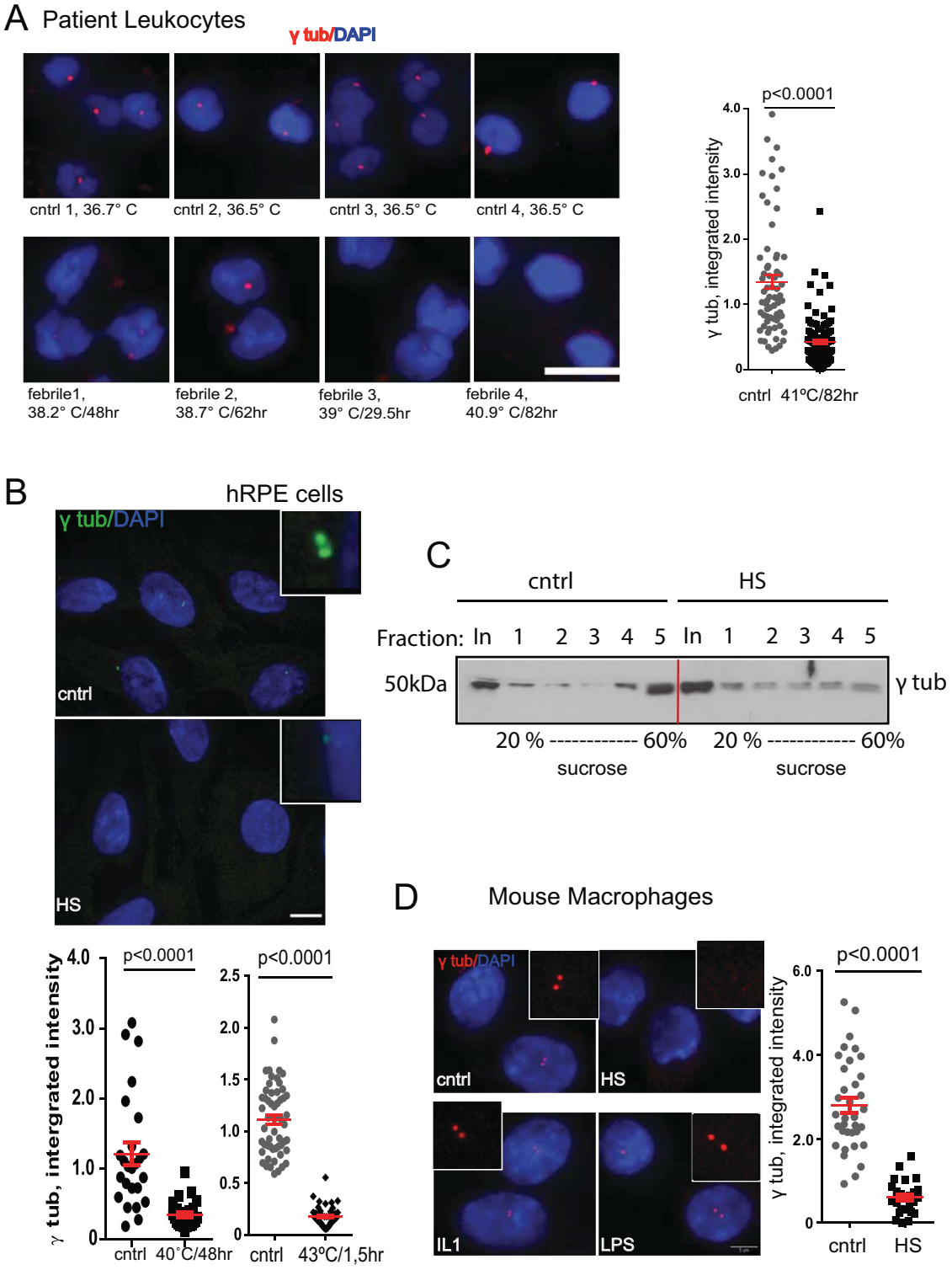

FIGURE 1: Elevated temperature in human febrile patients, primary mouse macrophages, and RPE cells leads to centrosome damage. (A) Comparison of γ-tubulin levels (red) in leukocyte centrosomes of febrile individuals (left, as indicated) and controls (left, top; cntrl); bar, 10 μm. Right, semiquantitative analysis of γ-tubulin signal intensity ($\times 10^5$ arbitrary units, $n = 60$–120 cells/sample, mean ± SEM, *t* test). (B) Images (cntrl and treated as indicated; inset, centrosomes), maximum projections; bar, 10 μm. Graphs, comparison of γ-tubulin at centrosomes in hRPE cells after exposure to the febrile patient temperature regimen (bottom, left) or HS (bottom, right), analyzed as in A. (C) Sucrose gradients of centrosomes from RPE cell control and HS lysates, separated by SDS–PAGE and immunoblotted for γ-tubulin. Fractions 4 and 5 indicate loss of centrosomal γ-tubulin from HS cells, whereas total (In, input) γ-tubulin is not decreased. (D) Images of γ-tubulin staining in primary mouse macrophages treated with HS, inflammatory cytokine interleukin-1 (IL-1), LPS, or control (cntrl, inset) centrosomes (bar, 5 μm). Right graph, semiquantitative analysis ($\times 10^5$ arbitrary units, $n = 25$–30 cells/sample, mean ± SEM).

both LPS and cytokines. We observed no decrease in γ-tubulin levels after exposure to either of these agents (Figure 1D). In contrast, cells exposed to HS underwent significant centrosomal γ-tubulin loss (Figure 1D). We conclude that elevated temperature alone is the likely cause of centrosome disruption in HS.

Heat stress disrupts molecular components of all centrosome substructures

To test the effects of HS on the centrosome, we analyzed molecular markers for several different centrosomal substructures, including the pericentriolar material (PCM; MT nucleation), mother and daughter centrioles, subdistal (MT anchoring) and distal appendages (ciliogenesis), and the centrosome linker protein rootletin. All PCM proteins tested (e.g., pericentrin [PCNT], PCM1, γ-tubulin; Figures 1 and 2A) were reduced at centrosomes. Centriole integrity was disrupted based on the reduction of centriole markers: Centrin2 (Figure 2B), glutamylated (stabilized) tubulin, SAS6, and Cep120 (Figure 2C). Consistent with the previously reported observation that centriole barrels are largely resistant to HS compared with PCM (Knox *et al.*, 1991), we found that the acetylated tubulin of the centrioles also remained unchanged during HS (Figure 2C). This indicated that microtubules modified by acetylation were heat resistant and might serve as a centrosome "remnant" for templating centrosome recovery. Indeed, centrosomes disrupted by HS returned to normal after ~24 h in normothermic conditions (see later, Figure 7A). Recoverability of damaged centrosomes suggests that the heat-induced centrosome inactivation is a dramatic but temporary event.

We also observed a decrease in the daughter centriole–specific marker centrobin (Figure 2F) and the appendage markers Cep83, ninein, p150, and cenexin at the mother centriole (Figure 2, B and D), suggesting that there was no discrimination between mother centriole and daughter centriole in terms of sensitivity to HS. Because cenexin is required for subdistal appendage formation (Ishikawa *et al.*, 2005) and Cep83 for distal appendage formation (Tanos *et al.*, 2013), their dramatic reduction at these sites indicates that both sets of appendages are lost or severely compromised. Similar results were obtained after HS of the centrosome linker protein rootletin (Bahe *et al.*, 2005; Figure 2E). Collectively these data demonstrate a reduction in molecular components of all centrosome substructures after HS.

Heat stress leads to loss of centrosome function

Global changes in centrosome composition suggested defects in its structure and function. One consequence of centrosome protein loss and compromised centrosome integrity after HS was a decrease in centrosomal MT organization and nucleation (Figures 2G and 3A), consistent with the loss of γ-tubulin, other PCM proteins (Figures 1B and 2A; Brown *et al.*, 1996), and ninein, a MT-anchoring protein (Figure 2B). HS also compromised primary cilia assembly from the mother centriole (Figure 3B), which is consistent with loss of markers for mother centriole (Figure 2, B and D). Important consequences of centrosome damage are mitotic defects (Figure 3C). Whereas the total number of cells in mitosis did not differ between control and stressed cells, further analysis of mitotic stages revealed that heat stress–exposed cells were found only in a prometaphase-like stage. Spindle poles were disrupted and no bipolar spindles were formed, so cells were not able to proceed to metaphase and were arrested in prophase, or cells that were heat stressed at metaphase experienced damaged spindles and loss of MT organization and therefore presented a prometaphase-like phenotype. HS also lead to defects in centrosome polarization toward the target during immunological synapse formation (Figure 3D). Collectively we refer to these heat-induced functional defects as centrosome inactivation.

Centrosome disruption during HS is achieved by localized proteasome degradation

HS-induced damage appears to result from protein denaturation and disruption. Misfolded proteins can aggregate, be refolded, or be degraded (Hartl *et al.*, 2011). Tests of these outcomes revealed centrosome-specific protein degradation as a primary mechanism of centrosome protein loss after HS (Figure 4). For example, cells pretreated with two different proteasome inhibitors, MG132 or lactocystin (LA), protected centrosome proteins compared with vehicle alone (Figure 4, A–C). The centrosome-specific increase in ubiquitinylation at the centrosome (Figure 4D), a modification that is often a prerequisite for protein degradation by the proteasome, is consistent with centrosome-specific degradation. Centrosomal localization of active proteasome subunits (Wigley *et al.*, 1999) also suggested that the centrosome itself might be the site of degradation. To test this more directly, we monitored proteasome activity using a proteasome reporter targeted directly to the centrosome (ubiquitin [Ub]-G76V-green fluorescent protein (GFP)-PACT; Puram *et al.*, 2013). Based on reporter activity, HS cells showed an increase in proteasome activity compared with controls (Figure 4E). We next took advantage of a centrosome-targeted proteasome ubiquitin receptor mutant (GFP-S5aC-PACT; Puram *et al.*, 2013) that lacks the N-terminal von Willebrand factor A, a domain required for binding proteins to the proteasome lid. We observed that γ-tubulin signals from HS cells expressing the mutant were increased at centrosomes, whereas the centrosome targeting sequence alone had no effect (Figure 4F). This indicated that the centrosome-associated proteasome is required for centrosome inactivation. It is also likely that other ubiquitin receptors act at the centrosome to facilitate proteasome activity. On the basis of these data, we suggest a novel function for the proteasomal machinery that is localized to the centrosome during HS, namely, the degradation of centrosome proteins.

Centrosome degradation during heat stress is specific

Of interest, centrosome disruption after HS appeared to be selective, as there was no detectable effect on the integrity of two nonmembranous organelles—the midbody and kinetochores—or on the membrane-bound organelles—mitochondria—after HS (Figure 5). For example, the mitochondrial markers ATP5A and mitochondrial Hsp70 showed no loss from mitochondria after HS (Figure 5A). Assessment of kinetochores in heat-stressed mitotic cells using CREST autoimmune serum and CenpE antibody showed no significant decrease in levels at kinetochores (Figure 5B). As we pointed out earlier, the mitotic progression of HS cells was impaired, and therefore we analyzed prometaphase-like cells based on the presence of CenpE. Note that the distribution of kinetochores was altered, most likely due to collapsed spindle poles and spindles (Figure 3C).

The canonical MB proteins mitotic kinesin-like protein and RacGAP showed no significant decrease from midbodies after HS (Figure 5, C and D). We next tested whether Septin7, which resides at both midbodies and centrosomes, was treated differently at these two different organelles after HS. Remarkably, we found that Septin7 was significantly diminished at centrosomes but unchanged at midbodies (Figure 5, E and F). This demonstrates that the same protein bound to different nonmembranous organelles in the same cell, at the same time, and under the same HS conditions was treated dramatically differently after HS. This result suggests that

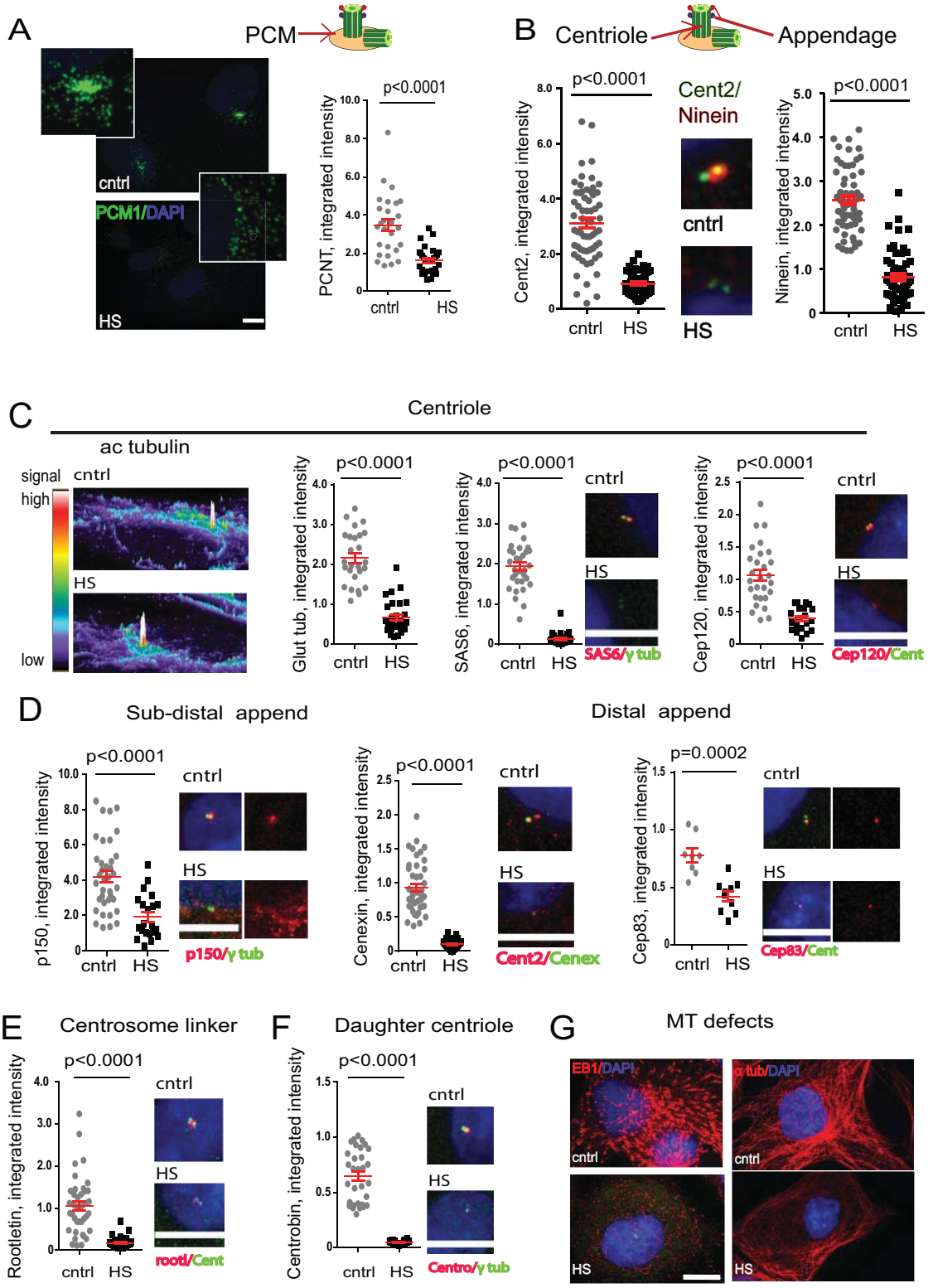

FIGURE 2: Centrosome defects during exposure to elevated temperature. (A) Maximum projections from confocal images of control and HS cells showing disruption of pericentriolar material marker PCM1; bar, 10 μm. Changes in PCNT are shown as semiquantitative analysis of integrated intensity ($\times 10^5$ arbitrary units, mean ± SEM). (B) Centrin2 (centriole marker, Cent2; left) and ninein (appendage marker, right) staining in RPE cells after HS (integrated intensity, $\times 10^5$ arbitrary units; $n = 40$–60 centrosomes/sample, mean ± SEM). Middle, maximum projections of centrosomes (Cent2, green; ninein, red). (C) Centriole integrity after HS based on intensity profiles of acetylated tubulin (left), glutamilated tubulin semiquantitative analysis of integrated signal intensity (middle left; $\times 10^6$ arbitrary units, mean ± SEM), SAS6 (middle right; $\times 10^5$ arbitrary units), and Cep120 (right; $\times 10^6$ arbitrary units); bar, 10 μm. (D) Signals of mother centriole markers p150, cenexin, and Cep83, respectively, are decreased in stressed cells; maximum projections of confocal microscope images of centrosomes (bar, 10 μm) and semiquantitative analysis of integrated intensity ($\times 10^5$ arbitrary

the centrosome responds to HS by degrading centrosome proteins, whereas the midbody remains unperturbed.

Recruitment of Hsp70 to the centrosome

Concurrent with centrosome disruption after HS was recruitment of the molecular chaperone Hsp70 to the centrosome (Figure 6, A and B, and Supplemental Figure S1A). Owing to the fact that many centrosome proteins use MT-based dynein-mediated transport to localize to the centrosome, we tested whether Hsp70 uses this mechanism for centrosome localization after HS. Despite HS-induced disruption of centrosomal MT organization (Figure 2G), nucleation (Figure 3A), and consequent loss of MT-based transport, Hsp70 localized to the centrosome (Figure 6, A and B, and Supplemental Figure S1A). To test more directly whether centrosome recruitment of Hsp70 was MT-dependent, we pretreated cells with the MT-depolymerizing agent nocodazole before HS. After HS, Hsp70 was recruited to the centrosome after MT depolymerization (Supplemental Figure S1B), demonstrating its independence of MTs.

We next tested whether PCNT, a protein of the outer layer of the PCM (Lawo *et al.*, 2012) and perhaps the first to make contact with Hsp70, interacted with Hsp70. We found that immunoprecipitation of Hsp70 coprecipitated PCNT (Figure 6C). Depletion of Hsp70 by RNA interference decreased centrosomal recruitment of Hsp70 after HS, as expected (Supplemental Figure S1A), and compromised the ability of centrosomes to recover from HS (Figure 7B). This is consistent with our earlier reciprocal experiment showing that global overexpression of Hsp70 protected centrosomes from HS damage (Brown *et al.*, 1996; Supplemental Figure S1, C and D). Taken together, these data demonstrate that Hsp70 is an essential centrosome protein during HS, interacts with the PCM component PCNT, and is critical for centrosome protection against HS.

Centrosome-targeted Hsp70 protects the molecular composition, structure, and function of centrosomes after HS

The data presented thus far demonstrate the protective effect of Hsp70 on the molecular integrity and function of centrosomes during HS. However, it is unclear whether the protective chaperone activity of Hsp70 acts directly on proteins at the centrosome or on centrosomal components within the cytoplasm to facilitate their recruitment back to centrosomes. To distinguish between these possibilities, we attempted to rescue heat-induced centrosome disruption by expressing Hsp70 fused to the centrosome-localizing PACT domain of PCNT (Gillingham and Munro, 2000) and to enhanced GFP (EGFP; centrosome-targeted Hsp70 [cHsp70]).

cHsp70 successfully targeted to the centrosome (Supplemental Figure S2, A and E) and did not affect endogenous Hsp70 expression (Supplemental Figure S2C) or localization of PCNT to centrosomes (Supplemental Figure S2D). Remarkably, stable expression of cHsp70 significantly prevented HS-induced centrosome disruption of γ-tubulin and Centrin2 at centrosomes (Figure 6, D and F, and Supplemental Figure S3A). In contrast, plasma membrane–targeted Hsp70 (mHsp70; Supplemental Figures S2, B and C, and S3A) was excluded from the centrosome (Supplemental Figure S2E) and failed to rescue HS-induced centrosome disruption (Figure 6, D and F); expression of the PACT domain alone (Supplemental Figure S3B) had no effect. Transient transfection of cells with cHsp70 confirmed results observed in stably expressing cHsp70 cells (Supplemental Figure S3, B and C).

Of importance, cHsp70 prevented defects in MT regrowth during HS (Figure 7C) and cilia formation (Figure 7D). These data demonstrate that the centrosomal pool of Hsp70 prevents centrosome disruption during HS, presumably by protecting proteins from denaturation that is likely induced by this process.

To test whether chaperone activity of cHsp70 was required for its protective function at the centrosome, we expressed a mutant form of cHsp70 lacking the ATP domain required for chaperone activity in RPE cells (D10S; cHsp70D10S; Rajapandi *et al.*, 1998). The mutant was targeted to the centrosome and subjected to HS. Centrosomal γ-tubulin levels in cells expressing the chaperone mutant were significantly lower than in cells expressing wild-type cHsp70 (Figure 6E), demonstrating an important role for the chaperone function of Hsp70 in preventing centrosome inactivation.

Pathological consequences of HS and their rescue by cHSP70

To test for potential pathological outcomes of centrosome inactivation after HS, we examined the immunological synapse. One function of this tight compartment between cells is to confine secreted molecules so they will only bind to and affect the cognate cell of the synapse. This critical function of the immunological synapse is controlled by the centrosome. To achieve this goal, the centrosome must move to and polarize toward the immunological synapse. This is followed by centrosome-dependent secretion of secretory granules to this site (Stinchcombe *et al.*, 2006). As in other cells that we tested, HS caused centrosome damage in the immunological synapse (Figure 3D), and the cHsp70 restored centrosome integrity, based on γ-tubulin signal, and partially rescued centrosome orientation (Figure 7F). A major pathological consequence of heat for the immunological synapse was the inability of the centrosome to polarize toward the target (Figure 3D). This can be explained by the observed loss of centrosomal astral MTs (Figures 2G and 3, A and D), which are required for centrosome polarization at the synapse (Yi *et al.*, 2013). Another consequence of HS at the immunological synapse was the inability of the centrosome to dock at the plasma membrane due to the loss of distal appendages, which are required for this process (Figure 2D; Tanos *et al.*, 2013). A final consequence of HS would be the inability to secrete vesicles at this site (Stinchcombe *et al.*, 2006), based on the aforementioned disruption of centrosome functions. Taken together, these data demonstrate important roles of the centrosome in immunological synapse function and highlight the consequences of their disruption.

DISCUSSION

This study shows that centrosomes are degraded during heat stress. We provide several lines of evidence that demonstrate centrosome degradation by the centrosomal fraction of the proteasome. These include increased ubiquitylation at centrosomes, degradation of a

units, mean ± SEM). (E) Changes in rootletin are shown as semiquantitative analysis of integrated intensity ($\times 10^6$ arbitrary units, mean ± SEM) and maximum projections of centrosomes from control and HS cells; bar, 10 µm. (F) Daughter centriole marker centrobin signal is decreased in stressed cells; maximum projections of confocal microscope images of centrosomes and semiquantitative analysis of integrated intensity ($\times 10^6$ arbitrary units, mean ± SEM). (G) Maximum projections from confocal microscopy images of growing ends of MTs from control and HS cells (DNA in blue, EB1 in red; bar, 10 µm) and maximum projections from confocal microscopy images of MTs from control and HS cells (DNA in blue, α-tubulin in red).

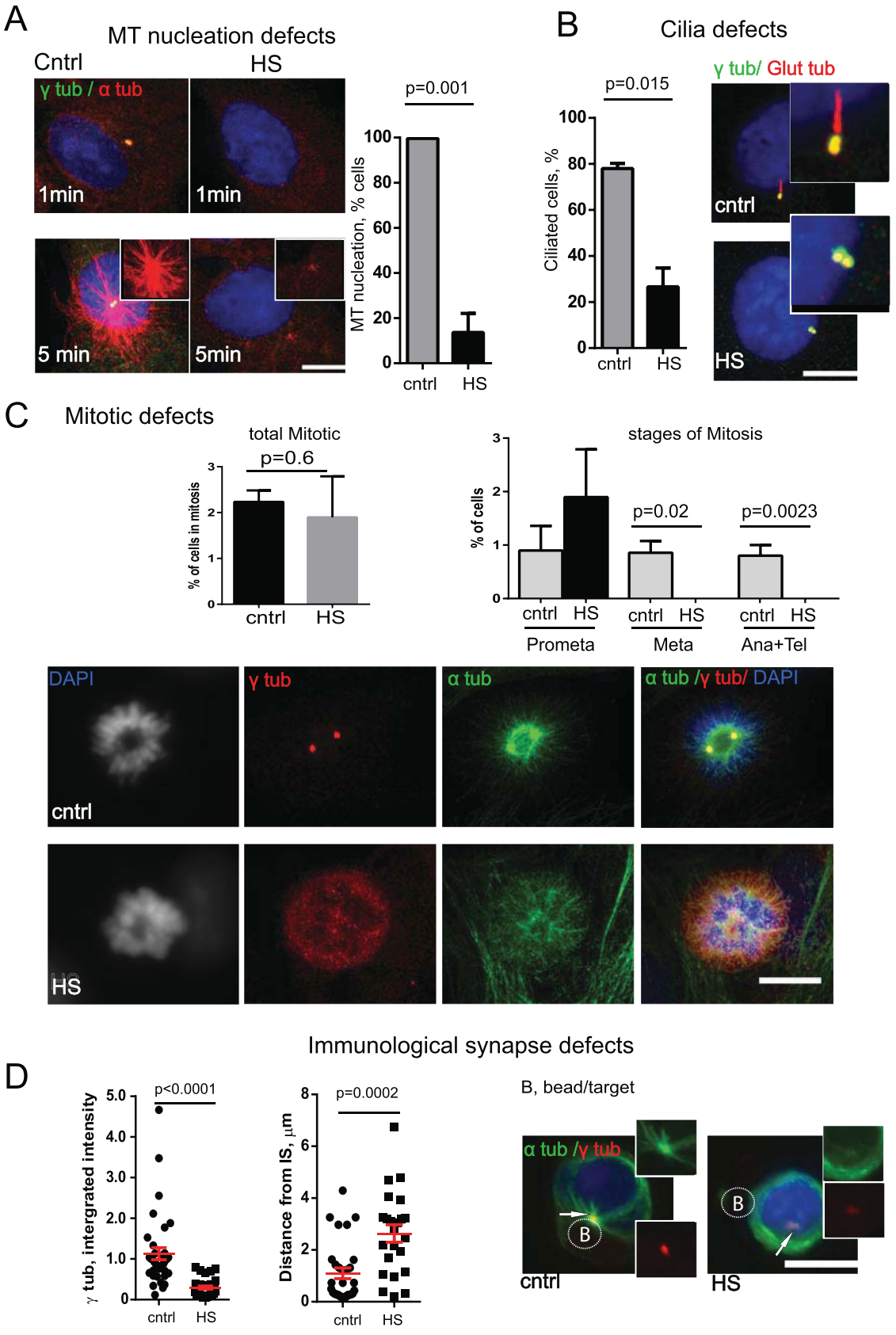

FIGURE 3: Consequences of centrosome damage. (A) MT nucleation 1 or 5 min after release from nocodazole treatment (α-tubulin, red; γ-tubulin, green) in control and HS RPE cells (bar, 10 µm). Right, percentage of cells with detectable MT nucleation at the centrosome at 1 min time point (three experiments, mean ± SD, *t* test). (B) Cilia formation is compromised after HS treatment (maximum projections; glutamylated tubulin, red; γ-tubulin, green); bar, 10 µm. Graph, percentage of ciliated cells (400–600 cells/experiment, three experiments, mean ± SD, *t* test). (C) Mitotic

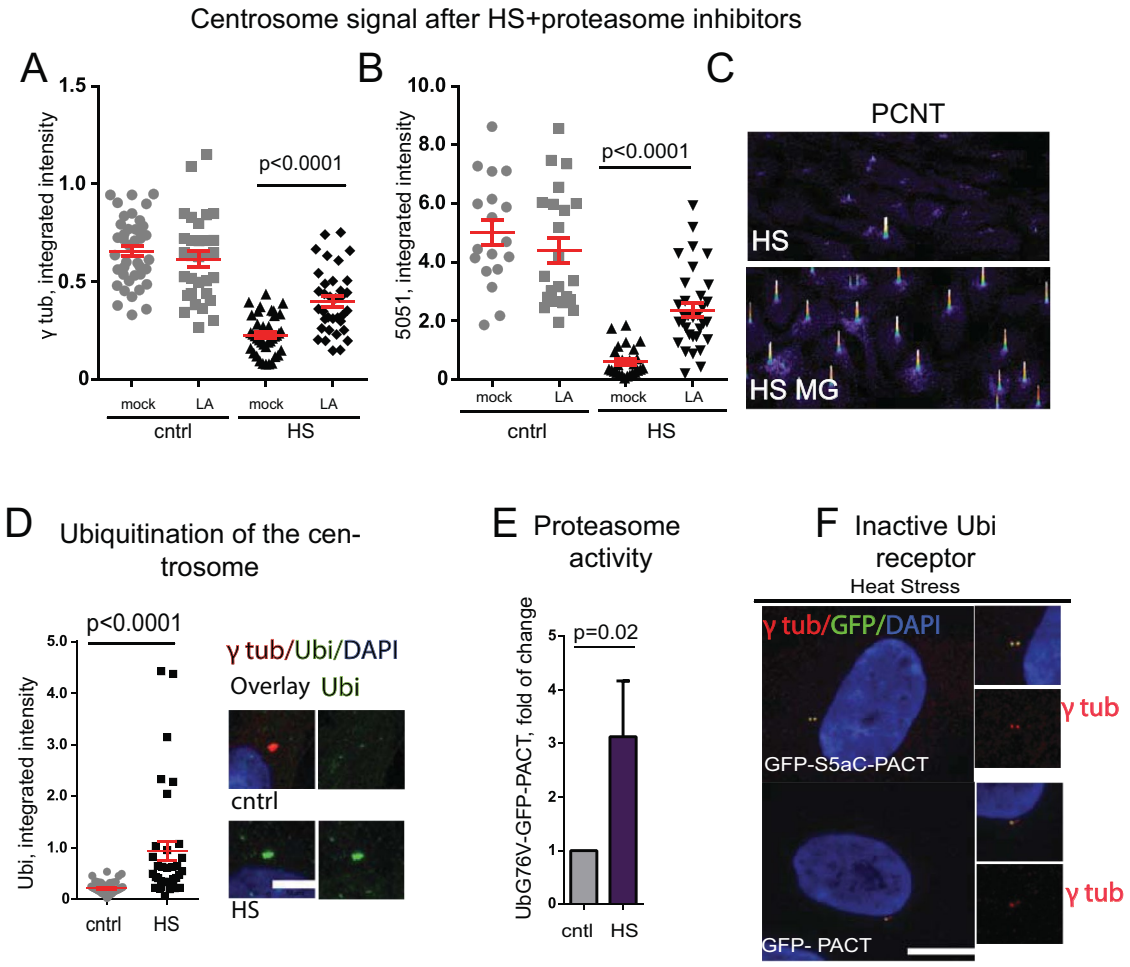

FIGURE 4: Heat stress triggers proteasome degradation of the centrosome. (A) Pretreatment with the proteasome inhibitor LA prevents γ-tubulin disruption upon HS; semiquantitative analysis of integrated intensity ($\times 10^5$ arbitrary units, mean ± SEM). (B) Loss of centrosome integrity based on 5051 marker, an autoimmune serum against centrosome that recognizes multiple centrosome proteins (Calarco-Gillam *et al.*, 1983), after HS is prevented by LA pretreatment. Semiquantitative analysis of integrated intensity ($\times 10^5$ arbitrary units, mean ± SEM). (C) Inhibition of the proteasome by MG132 prevents HS-induced disruption of the PCNT signal at the centrosome: semiquantitative intensity profiles of PCNT in HS cells or HS cells pretreated with MG132 for 1 h. (D) The ubiquitin signal (Ubi) is increased in HS centrosomes; maximum projections of microscope images of centrosomes (bar, 5 μm) and semiquantitative analysis of integrated intensity ($\times 10^5$ arbitrary units, mean ± SEM). (E) Proteasome activity at the centrosome after HS is increased threefold relative to activity at the centrosomes of control cells. Cells expressing the centrosome-targeted proteasome activity reporter Ub-G76VGFP-PACT were counted in cntrl and HS conditions; mean ± SD. (F) Maximum projections of confocal microscopic images of HS cells expressing either the dominant-negative mutant (GFP-S5aC-PACT) or GFP-PACT and immunostained for γ-tubulin (red). After HS, the centrosome is less disrupted in cells expressing GFP-S5aC-PACT than in GFP-PACT–expressing cells; bar, 10 μm.

Ub-conjugate reporter targeted to the centrosome, increased centrosome protein levels after exposure to two independent proteasome inhibitors, and expression of a centrosome-targeted Ub-receptor mutant that prevents binding to the proteasome lid and prevents degradation. This centrosome disruption pathway is selective in several ways. 1) Other types of stress do not induce centrosome inactivation (LPS, cytokines; 2) other nonmembranous and membrane-bound organelles, such as kinetochores, midbodies, and mitochondria, are not disrupted by HS; of interest, midbodies are degraded by autophagy rather than proteasome activity (Kuo *et al.*, 2011); and 3) a protein common to midbodies and centrosomes, Septin7, is lost specifically from centrosomes but not the

defects. Top left, percentage of cells in mitosis (three experiments, mean ± SD, *t* test). Top right, percentage of cells at different stages of mitosis (three experiments, mean ± SD, *t* test). Images, maximum projections of prometaphase cells, cntrl and HS, as indicated; bar, 10 μm. (D) HS leads to immune synapse (IS) defects. Left, γ-tubulin intensity is reduced at centrosome in HS-exposed Jurkat cell-CD3/28 bead conjugates ($\times 10^5$ arbitrary units, 20–40 centrosomes/sample, mean ± SEM, *t* test). Right, centrosome polarization toward IS is disrupted after HS exposure (distance between centrosome and IS [target bead] in micrometers). Images, maximum projections of Jurkat cell-CD3/28 bead conjugates stained with α-tubulin (green) and γ-tubulin (red) before and after HS show disruption in MT organization and centrosome damage; bar, 10 μm.

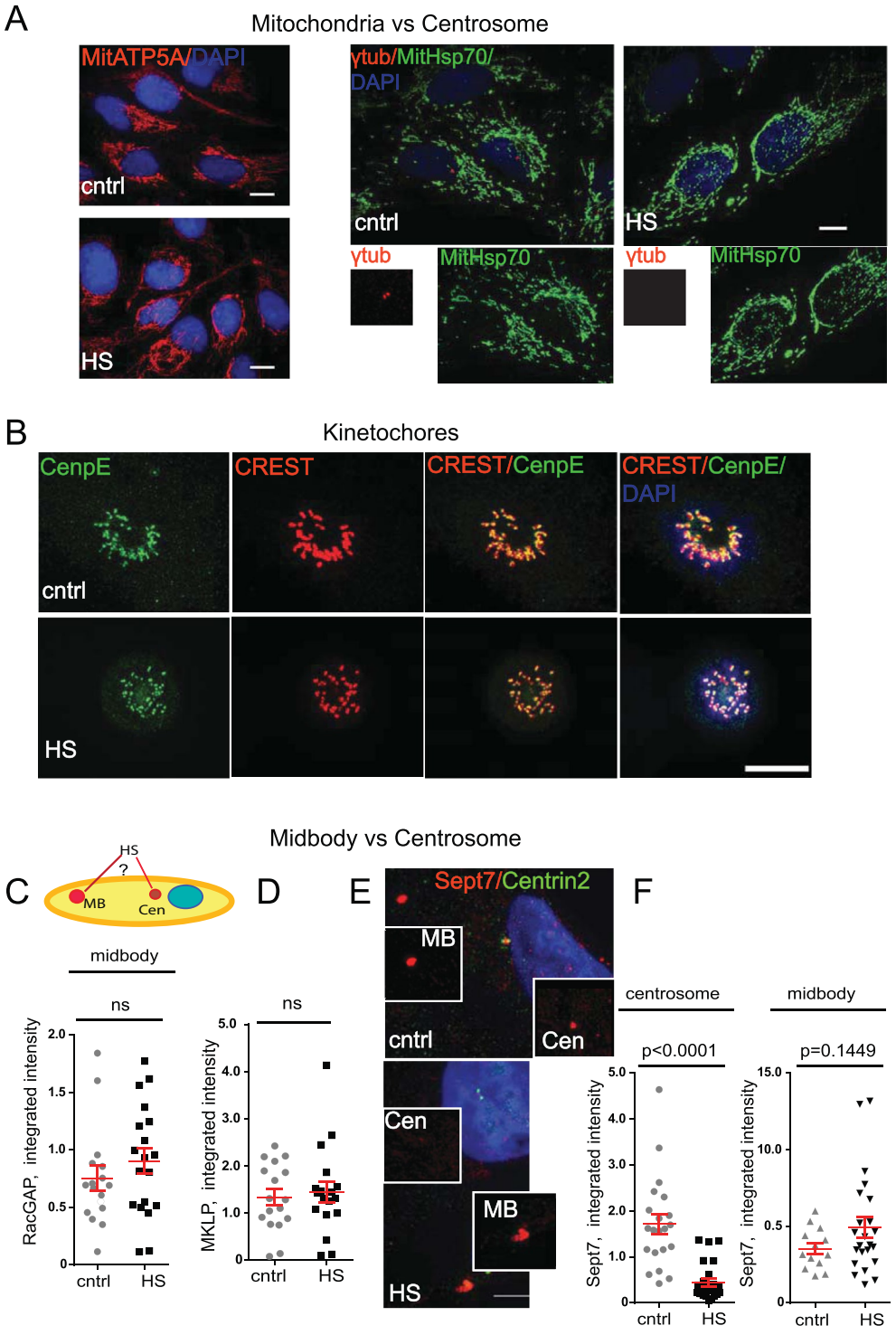

FIGURE 5: Centrosome degradation is specific. (A) Mitochondria are not degraded during HS. Maximum projections from confocal microscopy images show representative images of cntrl and HS cells immunostained with ATP5A (left; bar,10 μm) and mitochondrial Hsp70 (green) and γ- tubulin (red); middle and right, inset, centrosomes (bar, 10 μm). (B) Kinetochores are not degraded during HS. Maximum projections from confocal microscopy images show representative images of prometaphase cells from cntrl and HS cells immunostained with CenpE (green) and CREST (red); bar 10 μm. (C) Semiquantitative analysis of integrated intensity of the midbody marker RacGap ($\times 10^5$ arbitrary units, mean ± SEM) demonstrates no significant difference in signal intensity in HS cells. (D) Semiquantitative analysis of integrated intensity of the midbody marker mitotic kinesin-like protein ($\times 10^5$ arbitrary units, mean ± SEM) demonstrates no significant difference in signal intensity in HS cells. (E) Maximum projections from confocal microscopy images show representative images of cntrl and HS cells immunostained with Sept7 (red, decorates midbody, MB, and centrosomes, Cen) and Centrin2 (green, as centrosome marker); bar, 5 μm. HS results in loss of Septin7 from centrosomes but not from midbodies in the same cell. (F) Disruption of Septin7 signal after HS is shown at the centrosome but not at the midbody by semiquantitative analysis of integrated intensity ($\times 10^5$ arbitrary units, mean ± SEM).

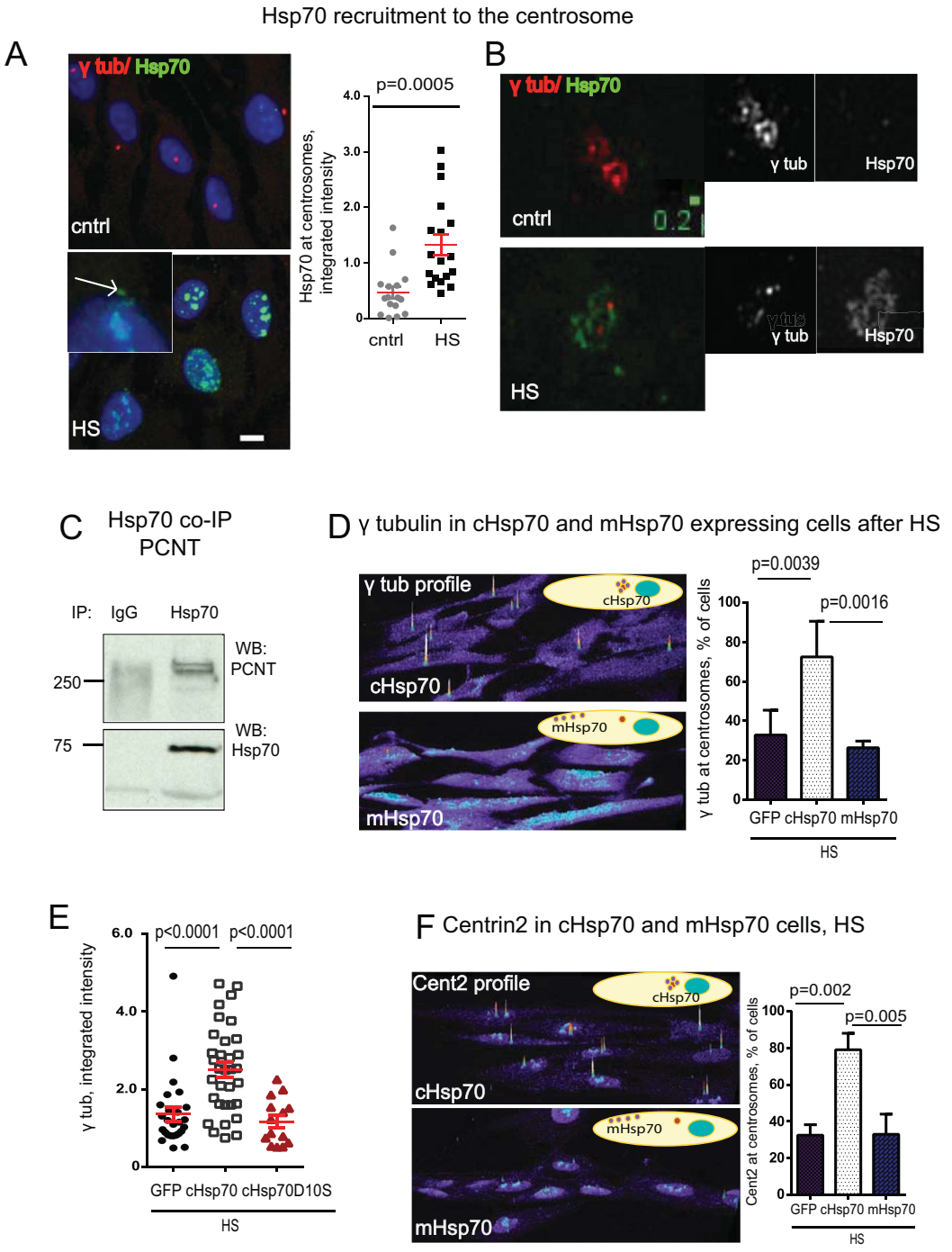

FIGURE 6: The centrosome is a substrate organelle for molecular chaperone Hsp70. (See also Supplemental Figures S1–S3.) (A) Left, images of maximum projections from cntrl and HS cells as indicated show that upon HS, Hsp70 accumulates at the centrosome and in the nucleus (inset, arrow points at the centrosome); bar, 10 μm. Semiquantitative analysis of integrated intensity ($\times 10^5$ arbitrary units) of centrosomal Hsp70 before and after HS (15–20 centrosomes/sample, mean ± SEM). (B) Superresolution images (OMX) demonstrate loss of γ-tubulin (red) from HS cells and recruitment of Hsp70 (green) as an outer layer in stressed cells; bar, 0.2 μm. (C) Immunoprecipitation (IP) of Hsp70 pulls down PCNT. Immunoglobulin G (IgG), control. (D) Centrosome-targeted Hsp70 (cHsp70) protects γ-tubulin from HS, whereas membrane-targeted Hsp70 (mHsp70) does not. Data are shown as semiquantitative profiles of confocal microscopy images. Right, percentage of cells with centrosomal γ-tubulin after HS in stably expressing centrosome-(cHsp70) or membrane-(mHsp70) targeted Hsp70-expressing cells (four experiments, 500–600 cells/sample, mean ± SD, one-way analysis of variance [ANOVA] combined with Tukey's multiple comparison test). (E) cHsp70, but not the chaperone-negative mutant cHsp70D10S, protects γ-tubulin signal at the centrosome; semiquantitative analysis of integrated γ-tubulin signal intensity ($\times 10^5$ arbitrary units, mean ± SEM). (F) cHsp70 protects centrosomal Centrin2 from HS, whereas mHsp70 does not. Data are shown as semiquantitative profiles of confocal microscopy images. Right, percentage of cells with centrosome-localized Centrin2 after HS in stably expressing cHsp70- or mHsp70-targeted Hsp70 cells (three experiments, 500–600 cells/sample, mean ± SD, one-way ANOVA combined with Tukey's multiple comparison test).

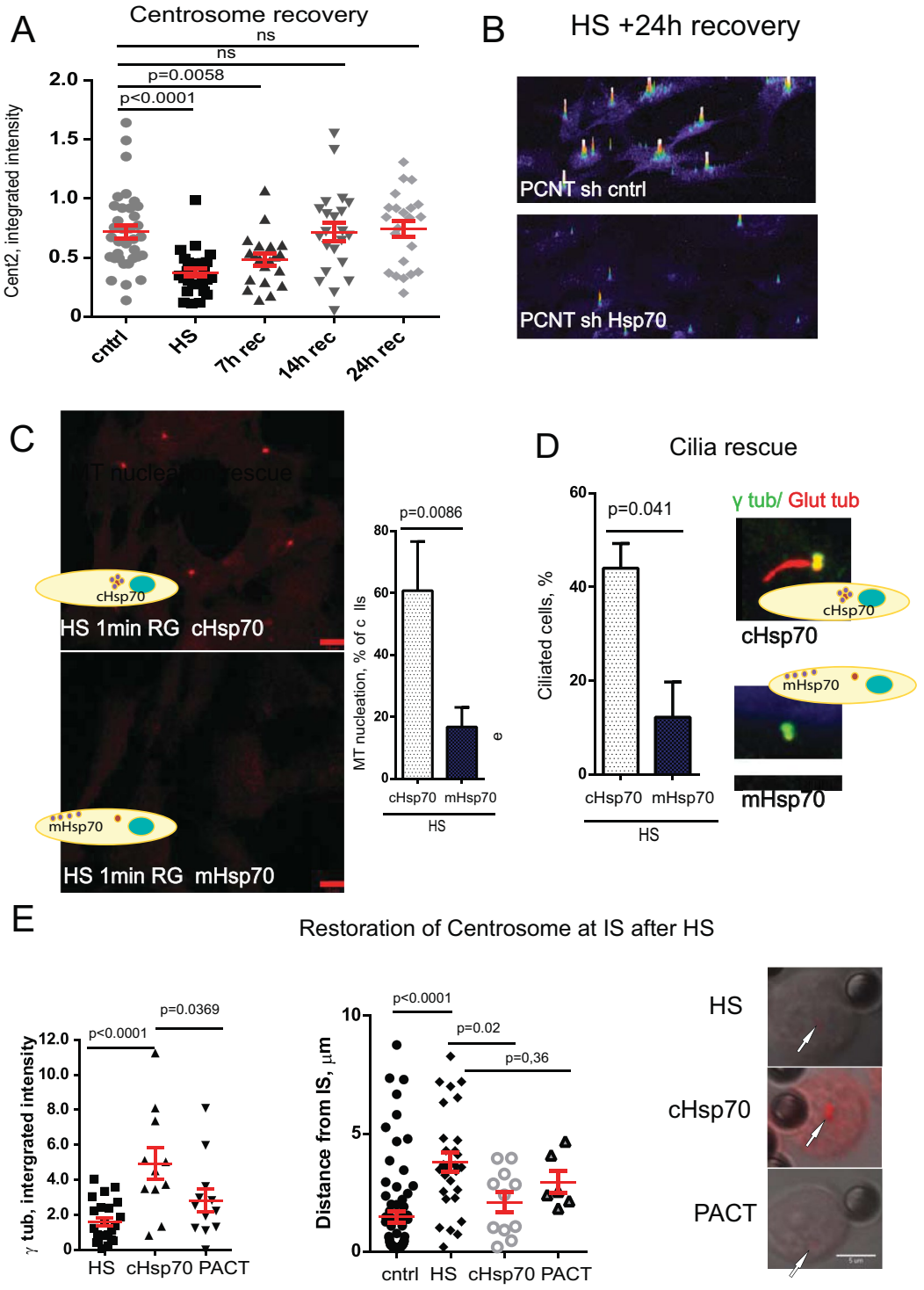

FIGURE 7: Hsp70 enables centrosome recovery, and protects centrosome functions after HS. (A) Semiquantitative analysis ($\times 10^5$ arbitrary units) of Centrin2 signal intensity shows centrosome disruption and recovery after HS during 24 h. (B) Semiquantitative intensity profiles of PCNT from cells recovered for 24 h at 37°C after HS demonstrate that Hsp70 depletion impairs centrosome recovery. (C) Confocal microscopy images demonstrating rescue of MT regrowth early after microtubule depolymerization (α-tubulin, 1 min of regrowth) after HS in cells expressing the centrosome targeting protein cHsp70 but not the membrane-targeting protein mHsp70. Percentage of the cells positive for detectable MT regrowth 1 min after HS exposure in RPE cell lines expressing cHsp70 or mHsp70 (five experiments, 400–500 cells/sample, mean ± SD). (D) Percentage of the cells with cilia after HS in cells expressing cHsp70 or mHsp70 (three experiments, 400–500 cells/sample, mean ± SD). Maximum projections of ciliated cells (cilia marker, glutamylated tubulin, red; centrosome marker, γ-tubulin, green) after HS exposure in cells expressing cHsp70 or mHsp70. (E) Centrosomal Hsp70 protects centrosome from HS-induced damage in IS conjugates; left, $\times 10^5$ arbitrary units, 10–40 centrosomes/sample, mean ±S EM; middle, distance between centrosome and IS, micrometers. Right, γ-tubulin, red, over DIC images; bar, 5 µm.

midbody after HS in the same cell, suggesting organelle specificity of the heat-induced degradation pathway.

It appears that several hours are required for centrosome restoration, which depends on the presence of the molecular chaperone Hsp70. Centrosome inactivation is prevented if active Hsp70 is targeted to the centrosome. This provides the evidence that the centrosome is a novel client organelle for Hsp70 and supports the idea that an entire organelle can be specifically maintained by Hsp70, as demonstrated for the lysosome (Kirkegaard *et al.*, 2010) and the nucleus (Kose *et al.*, 2012).

We propose a model in which centrosome function during HS involves a balance between proteasome degradation and Hsp70 chaperone activity, both acting at the centrosome. HS- and organelle-specific centrosome inactivation might be an adaptive response to stress, particularly critical for the immune response and, perhaps, preventing mitotic cells from further defects in DNA inheritance.

We also provide physiological evidence that centrosomes are disrupted in febrile individuals. Because fever often accompanies the immune response during inflammation (Hanson, 1997) and the centrosome plays a role at the immunological synapse (Stinchcombe *et al.*, 2006), the present study suggests that fever-induced centrosome defects have pathological consequences for the immunological synapse. During immunological synapse formation, the centrosome docks to the plasma membrane as it does during ciliogenesis (Stinchcombe *et al.*, 2006; de la Roche *et al.*, 2013). HS impairs cilia formation (Figure 3B) and cilia reabsorption (Prodromou *et al.*, 2012), induces centrosome degradation (Figure 4), and decreases the killing activity of cytotoxic leukocytes (Knox *et al.*, 1991). We demonstrate centrosome-associated defects in immunological synapse during HS (Figure 3D) and speculate that centrosome sensitivity toward elevated temperatures might be critical for immunological synapse function.

MATERIALS AND METHODS

Antibodies

The following antibodies were kind gifts: 20H5 Centrin2 (J. Salisbury, Mayo Clinic, Rochester, MN), polyglutamylated tubulin (GT335) antibody (P. Denoulet, College de France, Paris, France), and Cep120 (Zhigang Xie, Boston University, Boston, MA). The marker 5051 was described earlier (Calarco-Gillam *et al.*, 1983), and α-tubulin was produced in the lab from DM1alfa culture supernatant as described (Blose *et al.*, 1984). γ-Tubulin (AATR) was prepared as described (Zheng *et al.*, 1995). The following commercial antibodies were used: ninein (ab4447; Abcam [Cambridge, MA]), pericentrin (ab4448; Abcam), cenexin/ODF2 (ab43840; Abcam), centrobin (ab70448; Abcam), Hsp70 (SPA-810; Stressgen [Plymouth Meeting, PA]), PCM1 (5213; Cell Signaling [Danvers, MA]), glyceraldehyde-3-phosphate dehydrogenase (sc-32233; Santa Cruz Biotechnology [Dallas, TX]), rootletin (sc-67824; Santa Cruz Biotechnology), SAS-6 (sc-81431; Santa Cruz Biotechnology), Cep83 (HPA038161; Atlas [Stockholm, Sweden]), Septin7 (sc-20620; Santa Cruz Biotechnology), MLKP (sc-867; Santa Cruz Biotechnology), ubiquitin (550944; BD Transduction [San Jose, CA]), p150 (P50520-050; BD Biosciences), RacGAP (ab2270; Abcam), acetylated tubulin (T 6793; Sigma-Aldrich [St. Lous, MO]), EB1 (610534; BD Transduction), CREST (15-234-0001; Antibodies Incorporated [Davis, CA]), CenpE (ab5093; Abcam), ATP5A (ab14748; Abcam), mitochondrial Hsp70 (MA3-028; Affinity Bioreagents [Golden, CO]), GFP (DSHB-GFP-12A6; DSHB Biology [Iowa City, IA]), and GFP (sc-8334; Santa Cruz Biotechnology).

Corresponding secondary antibodies for immunofluorescence were conjugated with Alexa 568, Alexa 488, Alexa 647 (Invitrogen, Carlsbad, CA), Cy3, DyLight488, or DyLight 568 (Jackson ImmunoResearch, West Grove, PA). For Western blot, horseradish peroxidase anti-mouse and anti-rabbit secondary antibodies (Jackson ImmunoResearch) were used.

Constructs

GFP-S5aC-PACT and Ub-G76V-GFP-PACT plasmids were a kind gift from Albert Kim (Washington University School of Medicine, St. Louis, MO) and Azad Bonni (Harvard Medical School, Boston, MA). To create the cHsp70 construct, the mycPACT domain (from RFP-periCT1; a kind gift from Sean Munro) was inserted into EGF-PHsp70 (a kind gift from Andrew Judge [University of Florida, Gainesville, FL]) using *Bam*HI and *Xba*I. The stop codon at the end of the Hsp70 sequence was mutated (QuikChange; Stratagene) using the primer 5′-ccat tga gga ggt aga tgc agt cga cgg tac cgc gg and its complement.

The mHsp70 construct was created by inserting the myr-containing annealed duplex 5′/phos CTA GCA CCA TGG GGA GCA GCA AGA GCA AGC CCA AGA AA, 5′/phos-CCG GTT TCT TGG GCT TGC TCT TGC TGC TCC CCA TGG TG into EGFPHsp70 using *Nhe*I and *Age*I.

The chaperone-inactive centrosome-targeted Hsp70 was obtained by mutating D10S (Rajapandi *et al.*, 1998) residues in cHsp70 construct (QuikChange) using the forward primer 5′-gcc gcg gcg atc ggc atc agc ctg ggc acc acc and its complement.

Isolation of human white blood cells

Deidentified human blood samples from controls and patients (written consent was obtained at the Center for Conquering Disease, University of Massachusetts, Worcester, MA, before sample collection) were collected into EDTA-containing tubes, and white blood cells were isolated in accordance with standard procedures. Briefly, red blood cells were lysed by adding 2 ml of Lysis Buffer (BD) to 200 µl of whole blood and incubating for 15 min at room temperature, followed by centrifugation for 5 min at 1400 rpm. The pellet was resuspended in phosphate-buffered saline (PBS), spun onto a coverslip, and fixed with ice-cold methanol within 1 h after blood drawing.

Heat shock treatment, nucleation assay, and primary cilia formation

Cells were seeded onto coverslips 24 h before treatment, and, unless stated otherwise, heat shock was applied for 90 min at 43°C. For the microtubule regrowth assay, immediately after heat shock treatment or in control RPE cells, microtubules were depolymerized by 10–25 µM nocodazole in culture medium for 1 h at 37 °C. Cells were then washed three times with room temperature PBS and incubated in culture medium without nocodazole at 37 °C to allow nucleation. At the indicated time points, cells were fixed with methanol and processed for immunofluorescence microscopy to examine microtubule nucleation (α-tubulin). Primary cilia were induced by releasing control or heat-shocked cells into serum-free medium, for 24 h as described before (Prodromou *et al.*, 2012), cells were fixed with ice-cold methanol, and cilia were detected with GT335 antibody (Jurczyk *et al.*, 2004).

Immunological synapse formation assay

Jurkat cells were incubated with Human T-Activator CD3/CD28 Dynabeads (11161D; Invitrogen), using the manufacturer's protocol for 30 min to 2 h after HS treatment. Conjugates were isolated and fixed with ice-cold MeOH for at least 30 min before immunostaining.

Centrosome preparation

Centrosomes were isolated as described previously (Blomberg-Wirschell and Doxsey, 1998). Briefly, hRPE cells were incubated with culture medium containing 5 µg/ml cytochalasin D and 10 µg/ml nocodazole for 2 h at 37°C to depolymerize actin and microtubule filaments. Cells were briefly washed on ice with the following buffers: 1× PBS, 0.1× PBS, 8% (wt/wt) sucrose, 8% (wt/wt) sucrose in 1 mM Tris-HCl, 8 mM, and 2-mercaptoethanol followed by lysis with 1 mM Tris-HCl, 8 mM 2-mercaptoethanol, and 0.5% NP-40 (10 ml/plate) for 10 min with gentle rotation, and clarified by centrifugation for 3 min at 3000 rpm at 4°C. Supernatant was concentrated on 2 ml of 20% Ficoll cushion at 12,700 rpm for 15 min. Two milliliters of lysate was layered on the top of 20–62.5% sucrose gradient (prepared in 10 mM 1,4-piperazinediethanesulfonic acid, 1 mM EDTA, 1 mM Tris-HCl, 8 mM 2-mercaptoethanol, 0.1 Triton X-100) and centrifuged at 27,000 rpm (SW-28 rotor) for 2.5 h at 4°C. One-milliliter fractions were collected from the top of the gradient for further analysis by SDS–PAGE, followed by Western blot.

Immunostaining, microscopy, and software

Immunofluorescence microscopy analysis of −20°C methanol-fixed cells was carried out as previously described. Images were acquired with a Zeiss Axiovert 200M, a PerkinElmer Ultraview spinning disk microscope, and a Hamamatsu ORCA-ER camera (100×/numerical aperture [NA] 1.4 or 40×/NA 1.3 Plan-Apochromat oil objective). *Z*-stacks are shown as two-dimensional maximum projections (MetaMorph; Molecular Devices). Fluorescence range intensity was adjusted identically for each series of panels. Intensity profiles and fluorescence intensity quantification were obtained from sum projections of *Z*-stacks using MetaMorph. For fluorescence intensity quantification, computer-generated concentric circles of 60 (inner area) or 80 pixels (outer area) in diameter were used to measure centrosome (inner area) and calculate local background (difference between the outer and inner areas) fluorescence intensity.

Superresolution microscopy was performed as described earlier (Lawo *et al*., 2012) using a three-dimensional (3D) structured illumination microscope (SIM; OMX, Applied Precision). The 3D-SIM image stacks were reconstructed using SoftWoRx 5.0 software package (Applied Precision) and then imported into ImageJ (National Institutes of Health, Bethesda, MD) and projected using maximum intensity. All statistical analysis was done using GraphPad Prism software.

Cell culture, short hairpin RNAs, small interfering RNA, and transfections

Diploid human hTERT-RPE 1 cells (Clontech) and Jurkat cells were grown as recommended by the American Type Culture Collection. Primary LMEF (mouse embryonic fibroblasts) and macrophage cells were isolated by using standard procedures. Stable cell lines were created by nucleofecting (Lonza) hTERT-RPE1 cells with EGFP, cHsp70, and mHsp70 constructs. For Hsp70 depletion, RPE cells were transfected with shHsp70 (sense sequence, CGA CCT GAA CAA GAG CAT CAA) or siHsp70 (sense sequence, AGA ACC AGG TGG CGC TGA ATT).

Western blot and immunoprecipitation

Cells were lysed in ice-cold buffer (50 mM 4-(2-hydroxyethyl)-1-piperazineethanesulfonic acid, pH 7.5, 1 mM ethylene glycol tetraacetic acid, 150 mM NaCl, 1.5 mM $MgCl_2$, 10% glycerol, 1% IGEPAL, and proteinase inhibitors [Complete Mini; Roche Diagnostics]). Cell lysates were clarified at 13,000 rpm for 15 min at 4°C. Protein concentrations in lysates were assessed by the standard Bradford procedure and after, adjustment of loads, were subjected to SDS–PAGE and analyzed by Western blot. For immunoprecipitations, lysates were incubated with the indicated antibodies overnight at 4°C and then with G-PLUS agarose (Santa Cruz Biotechnology) for an additional 45 min, and then washed three times with lysis buffer and subjected to 12% SDS–PAGE, followed by Western blot.

ACKNOWLEDGMENTS

We express our thanks to Sarah Rulnick and Thomas Mayer (Center for Conquering Disease, University of Massachusetts, Worcester, MA) for obtaining human blood samples; Katherine Luzuriaga, Robin Brody, Linda Lambrecht, and Richard Hudson (University of Massachusetts, Worcester, MA) for help in isolating human white blood cells; Joel Richter and Sambra Redick for critical reading of the manuscript and continuous help; and Leanna Ferrand for help with the OMX imaging system. Research reported in this article was supported by the National Institutes of Health (RO1 GM051994-14 to S.J.D.) and the National Center for Advancing Translational Sciences of the National Institutes of Health under Award UL1TR000161. The content is solely the responsibility of the authors and does not necessarily represent the official views of the National Institutes of Health.

REFERENCES

Andrés-Delgado L, Antón OM, Alonso MA (2013). Centrosome polarization in T cells: a task for formins. Front Immunol 4, 191.

Bahe S, Stierhof Y-D, Wilkinson CJ, Leiss F, Nigg EA (2005). Rootletin forms centriole-associated filaments and functions in centrosome cohesion. J Cell Biol 171, 27–33.

Blomberg-Wirschell M, Doxsey SJ (1998). Rapid isolation of centrosomes. Methods Enzymol 298, 228–238.

Blose SH, Meltzer DI, Feramisco JR (1984). 10-nm filaments are induced to collapse in living cells microinjected with monoclonal and polyclonal antibodies against tubulin. J Cell Biol 98, 847–858.

Brown CR, Hong-Brown LQ, Doxsey SJ, Welch WJ (1996). Molecular chaperones and the centrosome. A role for HSP 73 in centrosomal repair following heat shock treatment. J Biol Chem 271, 833–840.

Bukau B, Weissman J, Horwich A (2006). Molecular chaperones and protein quality control. Cell 125, 443–451.

Calarco-Gillam PD, Siebert MC, Hubble R, Mitchison T, Kirschner M (1983). Centrosome development in early mouse embryos as defined by an autoantibody against pericentriolar material. Cell 35, 621–629.

Calloni G, Chen T, Schermann SM, Chang HC, Genevaux P, Agostini F, Tartaglia GG, Hayer-Hartl M, Hartl FU (2012). DnaK functions as a central hub in the E. coli chaperone network. Cell Rep 1, 251–264.

De la Roche M, Ritter AT, Angus KL, Dinsmore C, Earnshaw CH, Reiter JF, Griffiths GM (2013). Hedgehog signaling controls T cell killing at the immunological synapse. Science 342, 1247–1250.

Dinarello CA (2004). Infection, fever, and exogenous and endogenous pyrogens: some concepts have changed. J Endotoxin Res 10, 201–222.

Doxsey S, McCollum D, Theurkauf W (2005). Centrosomes in cellular regulation. Annu Rev Cell Dev Biol 21, 411–434.

Gillingham AK, Munro S (2000). The PACT domain, a conserved centrosomal targeting motif in the coiled-coil proteins AKAP450 and pericentrin. EMBO Rep 1, 524–529.

Hanson DF (1997). Fever, temperature, and the immune response. Ann NY Acad Sci 813, 453–464.

Hartl FU, Bracher A, Hayer-Hartl M (2011). Molecular chaperones in protein folding and proteostasis. Nature 475, 324–332.

Ishikawa H, Kubo A, Tsukita S, Tsukita S (2005). Odf2-deficient mother centrioles lack distal/subdistal appendages and the ability to generate primary cilia. Nat Cell Biol 7, 517–524.

Jurczyk A, Gromley A, Redick S, San Agustin J, Witman G, Pazour GJ, Peters DJM, Doxsey S (2004). Pericentrin forms a complex with intraflagellar transport proteins and polycystin-2 and is required for primary cilia assembly. J Cell Biol 166, 637–643.

Kirkegaard T, Roth AG, Petersen NHT, Mahalka AK, Olsen OD, Moilanen I, Zylicz A, Knudsen J, Sandhoff K, Arenz C, *et al.* (2010). Hsp70 stabilizes lysosomes and reverts Niemann-Pick disease-associated lysosomal pathology. Nature 463, 549–553.

Knox JD, Mitchel RE, Brown DL (1991). Effects of hyperthermia on microtubule organization and cytolytic activity of murine cytotoxic T lymphocytes. Exp Cell Res 194, 275–283.
Kose S, Furuta M, Imamoto N (2012). Hikeshi, a nuclear import carrier for Hsp70s, protects cells from heat shock-induced nuclear damage. Cell 149, 578–589.
Kuo T-C, Chen C-T, Baron D, Onder TT, Loewer S, Almeida S, Weismann CM, Xu P, Houghton J-M, Gao F-B, *et al*. (2011). Midbody accumulation through evasion of autophagy contributes to cellular reprogramming and tumorigenicity. Nat Cell Biol 13, 1214–1223 [correction published in Nat Cell Biol (2011), 13, 1467].
Lawo S, Hasegan M, Gupta GD, Pelletier L (2012). Subdiffraction imaging of centrosomes reveals higher-order organizational features of pericentriolar material. Nat Cell Biol 14, 1148–1158.
Okiyoneda T, Barrière H, Bagdány M, Rabeh WM, Du K, Höhfeld J, Young JC, Lukacs GL (2010). Peripheral protein quality control removes unfolded CFTR from the plasma membrane. Science 329, 805–810.
Prodromou NV, Thompson C, Osborn DPS, Cogger KF, Ashworth R, Knight MM, Beales PL, Chapple JP (2012). Heat shock induces rapid resorption of primary cilia. J Cell Sci 125, 4297–4305.
Puram SV, Kim AH, Park HY, Anckar J, Bonni A (2013). The ubiquitin receptor S5a/Rpn10 links centrosomal proteasomes with dendrite development in the mammalian brain. Cell Rep 4, 19–30.
Rajapandi T, Wu C, Eisenberg E, Greene L (1998). Characterization of D10S and K71E mutants of human cytosolic Hsp70. Biochemistry 37, 7244–7250.
Stinchcombe JC, Majorovits E, Bossi G, Fuller S, Griffiths GM (2006). Centrosome polarization delivers secretory granules to the immunological synapse. Nature 443, 462–465.
Tanos BE, Yang H-J, Soni R, Wang W-J, Macaluso FP, Asara JM, Tsou M-FB (2013). Centriole distal appendages promote membrane docking, leading to cilia initiation. Genes Dev 27, 163–168.
Vidair CA, Doxsey SJ, Dewey WC (1993). Heat shock alters centrosome organization leading to mitotic dysfunction and cell death. J Cell Physiol 154, 443–455.
Wigley WC, Fabunmi RP, Lee MG, Marino CR, Muallem S, DeMartino GN, Thomas PJ (1999). Dynamic association of proteasomal machinery with the centrosome. J Cell Biol 145, 481–490.
Willmund F, Del Alamo M, Pechmann S, Chen T, Albanèse V, Dammer EB, Peng J, Frydman J (2013). The cotranslational function of ribosome-associated Hsp70 in eukaryotic protein homeostasis. Cell 152, 196–209.
Yi J, Wu X, Chung AH, Chen JK, Kapoor TM, Hammer JA (2013). Centrosome repositioning in T cells is biphasic and driven by microtubule end-on capture-shrinkage. J Cell Biol 202, 779–792.
Zheng Y, Wong ML, Alberts B, Mitchison T (1995). Nucleation of microtubule assembly by a gamma-tubulin-containing ring complex. Nature 378, 578–583.